Application of DORT to Active Sonar

Charles F. Gaumond, David M. Fromm,
Joseph Lingevitch, Richard Menis,
Geoffrey Edelmann, David Calvo, & Elisabeth Kim,
Naval Research Laboratory
4555 Overlook Avenue SW
Washington, DC, 20375-5320, USA
charles.gaumond@nrl.navy.mil

Abstract **- Active sonar in shallow water is often reverberation-limited and the detectability is often limited by the presence of too many false alarms. The problem of improving detection, and classification, in shallow water is being worked on in several different ways. The Time Reversal Operator Decomposition (DORT) is a technique that has recently been applied to the problem of discriminating echoes in shallow water based on the different depths of the scatterers. DORT uses scattering data from a multiple source and multiple receiver sonar arrangement to separate scatterers that are resolvable by the source and receiver arrays. DORT is the application of the singular value decomposition of the frequency-domain data.**

This paper presents a derivation of DORT from the sonar equation. DORT is inherently a frequency-domain technique. In order to preserve range-resolution, the sonar equation is transformed into the time-frequency domain. With that representation, DORT can be applied to the frequency domain signal within a range resolution cell.

Following the derivation of DORT from the sonar equation, numerical simulations are shown that demonstrate the depth resolution of a vertical line array of sources and receivers. Sufficient depth resolution is shown using few sources at frequencies near 500 Hz in water with a depth of 100 m.

Problems that are encountered with the implementation of the technique are discussed. Target motion causes leakage of signal energy into several singular values. Motion of the source or receiver are shown to have little effect. The problems and constraints that arise from different multiplexing techniques, including frequency, code and time division, are shown. Results are shown with data taken on the Atlantic shelf, east of Cape May, NJ, during Geoclutter 03 and TREX-04 experiments.[1]

I. INTRODUCTION

Recently, advances have occurred in the use of time reversal in ultrasonic systems notably the development of Time Reversal Operator Decomposition (DORT) [1]. DORT can be used to analyze mathematically the process of iterative time reversal that eventually focuses on the strongest scatterer. More importantly, DORT allows the simultaneous determination of all the resolved scatterers from an analysis of the scattering matrix, or T-matrix.

Several approaches to applying the DORT technique have been published [2,3,4] and presented [5,6,7,8,9]. This paper addresses the use of DORT as a possible tool to enhance the detection of a scatterer located in the water column in the presence of noise and bottom reverberation.

This paper is organized as follows. First a brief description of our sonar signal model is given. Then a theoretical description of DORT signal processing as applied to the sonar system is given. After that, results of the sea test are shown. Finally, a conclusion and summary are given.

II. THEORY

A. Signal Model

Consider the development of a matrix of data. A set of source elements individually transmit a signal and each receiver element records the signal resulting from each transmission. The signal model is the well-known sonar equation in the time domain — where $p\left(\vec{r}_R,\vec{r}_S,t\right)$ is the pressure at position $\vec{r}_R$ in the water column that is caused by the S^{th} source transmission, $g(\vec{r}_R,\vec{r}_i,t)$ is the propagation Green's function from position $\vec{r}_i$ to $\vec{r}_R$, $a_i(t)$ is the time-response of the ith small scatterer, and $s(\vec{r}_S,t)$ is the transmitted signal at source potion $\vec{r}_S$ —

$$p(\vec{r}_R,\vec{r}_S,t)= \sum_i g(\vec{r}_R,\vec{r}_i,t)*a_i(t)*g(\vec{r}_i,\vec{r}_S,t)*s(\vec{r}_S,t)+n_S\left(\vec{r}_R,t\right). \quad (2.1)$$

Note that the noise signal $n_S\left(\vec{r}_R,t\right)$ has a subscript of the source index to denote the recording of an independent realization of noise at each source transmission. Also note that the scatter can be either in the water column or distributed along the bottom.

B. DORT in the Frequency Domain

If we assume that the Green's function and scatterer response are time invariant, the frequency domain transform of (2.1) is

$$P(\vec{r}_R,\vec{r}_S,f)= \sum_i G(\vec{r}_R,\vec{r}_i,f)A_i(f)G(\vec{r}_i,\vec{r}_S,f)S(\vec{r}_S,f)+N_S\left(\vec{r}_R,f\right). \quad (2.2)$$

We constrain the analysis to the frequency band of the LFM source signal and match filter the data (with a unit amplitude filter) to produce the following matrix equation

$$P_{RS} = G_{RI}A_{II}G_{IS}S_0 + N_{RS}, \quad (2.4)$$

where S_0 is the scalar transmitted source level.

We consider this signal in two limiting cases, one noise-dominant and the other signal-dominant, and a third mixes-case.

[1] This research was funded by ONR.

C. Signal Dominant Case

The form of the signal-dominant case

$$\mathbf{P} = \mathbf{G}^R \mathbf{A} \mathbf{G}^S S_0 , \tag{2.5}$$

resembles the singular value decomposition of the pressure data matrix

$$\mathbf{P} = \mathbf{U}\mathbf{S}\mathbf{V}^T , \tag{2.6}$$

where **T** denotes the complex conjugated transpose. By definition, the singular vector matrices are orthogonal. The Green's function vectors are also orthogonal, namely the product $\mathbf{G}^R\mathbf{G}^{R\dagger}$ is diagonal, if the scatters are resolved. In other words, scatterers are resolved if the array is able to focus sound on each scatterer independently. The resolution obviously depends on the environment and positions of the sources and receivers.

This implies that there is a connection between the nth individual scatter and one of the singular components, which we enumerate as the nth, of the data matrix, namely,

$$G_{Rn} A_{nn} G_{nS} S_0 = U_{Rn} S_{nn} V_{nS}^T . \tag{2.7}$$

A back-propagation image can be generated in the frequency domain using a single component of the SVD by multiplying on the left and right by the propagating Green's function. This results in a function of space and frequency:

$$I_B(\vec{r}_k, f) = G_{kR}^T G_{Rn} A_{nn} G_{nS} G_{Sk}^T S_0 . \tag{2.8}$$

If (2.8) is inverse Fourier transformed into time, then

$$i_B(\vec{r}_k, t) = g_{kRn}(t) * a_n(t) * g_{nSk}(t) * s_0(t) , \text{ where} \tag{2.9}$$

$$g_{kRn}(t) = g^*\left(\vec{r}_k, \vec{r}_R, t\right) * g\left(\vec{r}_R, \vec{r}_n, t\right) \text{ and} \tag{2.10}$$

$$g_{nSk}(t) = g\left(\vec{r}_n, \vec{r}_S, t\right) * g^*\left(\vec{r}_S, \vec{r}_k, t\right) . \tag{2.11}$$

Thus the time-domain back-propagation image equals the convolution of several terms. When the image is evaluated at the position of the scatterer, then the image equals the product of 1) the sum of the autocorrelations of the propagation from the receiver elements to the target position with 2) the target response function and with 3) the sum of the autocorrelations of the propagation from the source elements to the target position. Because the propagation autocorrelations are strictly real, the resulting time functions are centered at and symmetric about the origin. Any deviation from symmetry is due to the temporal response of the target.

The ability to form the back-propagation image depends on the availability of a sufficiently accurate propagating Green's function. If the environment is not known, then back-propagation images cannot be made. However a very limited form of back-propagation can be performed using only the **U** and **V** matrices. Multiplication by **U** and **V** can be interpreted as a back-propagation to the position of the scatterer using the following argument.

Note that if **G** is evaluated at the position of the scatterer, then the propagation vectors G_{Rn} and singular vectors U_{Rn} are respectively parallel so that

$$U_{Rn} = G_{Rn} \Big/ \left\| G_{Rn} \right\| \tag{2.12}$$

— and likewise — with **V** to within a phase shift that depends on the average phases of the two propagator vectors, the phase of the target response and the SVD algorithm. Therefore using (2.7), (2.8) and (2.12),

$$S_{nn} = \left| I_B \right| \Big/ \left(\left\| G_{Rn} \right\| \left\| G_{nS} \right\| \right) , \text{ or} \tag{2.13}$$

$$S_{nn} = G_{nR}^T G_{Rn} \left| A_{nn} \right| G_{nS} G_{Sn}^T \left| S_0 \right| \Big/ \left(\left\| G_{Rn} \right\| \left\| G_{nS} \right\| \right) , \tag{2.14}$$

which shows how the singular value is related to two transmission losses, the source level and the target response. After $S_{nn}(f)$ is inverse Fourier transformed the resulting time function $s_{nn}(t)$ is not as simply related to physical quantities as the time domain image, but is related to the convolution of the autocorrelations of the propagation and target response. Because $S_{nn}(f)$ is real by definition of the SVD, $s_{nn}(t)$ is symmetric about the origin of time. The time behavior of $s_{nn}(t)$ can be expected to reflect the spreading due to propagation and target response.

D. Noise Dominant Case

In the noise dominant case the data matrix is a matrix of random numbers

$$\mathbf{P} = \mathbf{N} , \tag{2.15}$$

that has a singular value spectrum that depends on the particular statistics and size of the matrix. Note that the expected values of the singular values are not equal; the values decay gradually with increasing singular index.

The SVD of random matrices, with independent Gaussian elements, are averaged and the mean normalized squared singular values given in Table 1. Theories of the spectra of random matrices have been studied [10]. The results in Table 1 were generated numerically and are accurate to two significant figures.

TABLE I
Normalized Singular Values of Random Matrices

Dimension	Singular values
[4, 56]	[0.34 0.27 0.22 0.17]
[5, 56]	[0.29 0.24 0.19 0.16 0.12]
[6, 56]	[0.26 0.21 0.17 0.15 0.12 0.09]

Of course, the singular values derived from a matrix, where the statistics are not Gaussian and the elements are not independent, would differ from those in Table 1. If there were a component of the noise that originated in a particular direction, then the singular values would show that by concentrating that energy into a single singular value.

E. Signal Plus Noise Case

Consider a data matrix that is composed of a rank-1 signal matrix and a full rank noise matrix,

$$\mathbf{P} = \mathbf{U}_1 S_0 \mathbf{V}_1^T + \mathbf{N} , \tag{2.16}$$

where $\mathbf{U}_1$ and $\mathbf{V}_1$ are normalized column vectors, S_0 is the scalar signal level and **N** is the noise data matrix as in (2.15) with a Frobenius norm $\|\mathbf{N}\|$. The SVD of the data matrix, with the signal and noise matrices being Gaussian random variables, is computed and the average found. The resulting squared average singular values are plotted using two different normalizations. (Note that the singular values are plotted with respect to the ratio $\mathrm{SNR}/(1+\mathrm{SNR})$ so that

both asymptotes – full signal and full noise – can be shown easily.) In Fig. 1, the normalization is by S_0, the Frobenius norm of the signal matrix. Note that the largest singular value is roughly constant for large values of SNR where it is dominated by the signal. At SNR = 1, the signal singular value has been increased by less than 1 dB by contamination with noise.

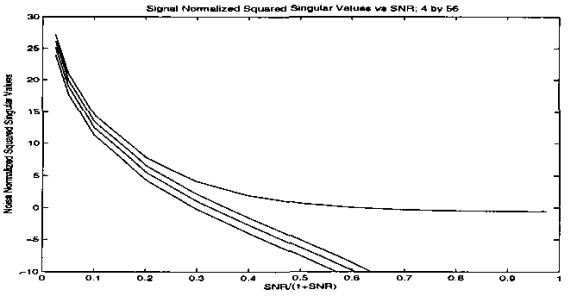

Fig. 1. Signal-normalized singular values of a data matrix of dimension (4,56) with a rank-1 signal and full rank Gaussian noise.

The singular values shown in Fig. 2 have been normalized by $\|N\|$. Thus the lowest three singular values, which correspond mostly to the noise, have nearly constant value as a function of SNR, while the highest singular value, which corresponds mostly to the rank-1 signal, increases with increasing SNR.

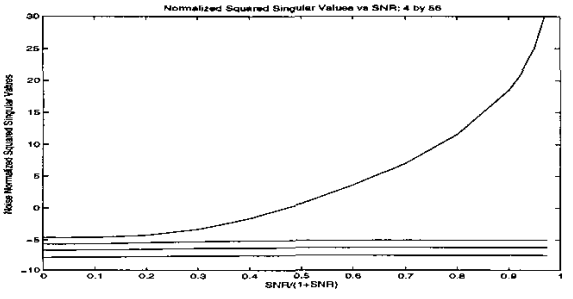

Fig. 2. Noise-normalized Singular values of a data matrix of dimension (4,56) with a rank-1 signal and full rank Gaussian noise.

These two figures show how the signal and noise singular values are mixed at various SNR. Fig. 1 shows that the signal singular value is increased by less than 1 dB at SNR = 1. Fig. 2 shows that the lowest three noise singular values are effected very little by the rank-1 signal.

F. Time Frequency Domain

In a sonar system, several problems can arise in the application of DORT. One of the simplest to overcome is the presence of more than one scatterer at different ranges. If range separation is resolved by the transmitted signal and the spreading of the channel, then the echo from each scatterer can be time-windowed and analyzed separately. This separation can be implemented by using the time-frequency domain with a sequence of analysis-windows that obey

$$1 = \sum_m w(t - mT), \tag{2.17}$$

where T is the time shift associated with the window and m is the epoch. The windows can be overlapping – e.g., 50% overlapping triangular window – or not – a rectangular window – and the condition still met.

Applying the time window decomposition yields a data matrix with indices of receiver, source, epoch and time. A Fourier transform over time (namely the "short time" and not "long time" or epoch) yields a data matrix with indices of receiver, source, epoch and frequency. The DORT algorithm is then applied to each epoch and frequency independently,

$$d(R,S,m,t) = p\left(\vec{r}_R, \vec{r}_R, t\right) w(t - mT), \tag{2.18}$$

$$D(R,S,m,f) = \sum_n U(R,n,m,f) S(n,m,f) V^T(n,S,m,f). \tag{2.19}$$

This yields a set of singular values at each epoch and frequency, namely $S(n,m,f)$ where n is the singular index, m the epoch index and f the frequency index.

Remembering that $S(n,m,f)$ is proportional to the back propagation image focused on the position of the target as shown in (2.13), the inverse Fourier transform $s(n,m,t)$ is related to the impulse response of the target convolved with the autocorrelations of the propagation to the target from the source and from the receiver.

III. Experiment

A. Description of experiment

The Time Reversal EXperiment TREX-04 was performed southwest of the Hudson Canyon on the 94 m bathymetry contour from April 22 to May 4, 2004, with two ships, the R/V Cape Henlopen and R/V Endeavor. The moored Cape Henlopen deployed the 64-element Source Receiver Array (SRA) vertically suspended from the A frame on the stern. The drifting R/V Endeavor deployed the echo repeater, which used either a single Raytheon XF4 or an ITC200 source. The XF4 was used for frequencies from 500 to 2500 Hz. The ITC covered the band from 2500 to 3500 Hz. The data shown here was taken on Julian Day 122 and 123.

B. Transmitted signal sequences

The success of the utility of DORT relies on the ability to record echoes from a sequence of independent source transmissions. The source, target, receiver and environment cannot change appreciablely during that sequence of recordings. Changes erode the rank-1 structure of the echo from an isolated target. There are several ways to transmit this sequence, such as critically spaced frequencies [6] or Code Division Multiple Access (CDMA). In this paper we report on the four transmission sequences in Table II. These are time-delayed sequences with very short time intervals to achieve sufficient time-invariance. The use of a broadband signal allows the evaluation of propagation spreading effects. The time-delayed sequence allows an evaluation of the erosion of time-invariance over the duration of the sequence.

The first and third consist of a sequence of broadside transmissions from the array. The echoes from these signals should be identical if there is time-invariance over the one second duration (namely 4 x 250 ms) of the sequence. The second and fourth consist of four distinct angles and are sufficient for performing DORT.

TABLE II Transmission Sequences					
#	Frequency (kHz)	Type	Duration (ms)	Spacing (ms)	Angle (+deg=up)
1	0.5 – 1.0	LFM	250	250	[0 0 0 0]
2	0.5 – 1.0	LFM	250	250	[5 0 -5 -10]
3	3.0 – 3.5	LFM	250	250	[0 0 0 0]
4	3.0 – 3.5	LFM	250	250	[5 0 -5 -10]

C. Numerical Simulation

Fig 3 shows the transmission loss from a numerical simulation of the 0.75 kHz sound emitted from 0, 5, -5, and -10 deg beams from the 64-element array. Note that the four beams ensonify the water column very differently and therefore produce four independent sets of data.

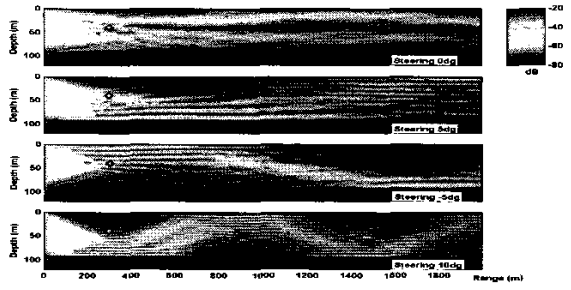

Fig. 3. Transmission loss from 0° (top), 5°, -5° and -10° (bottom) beams.

The resolution of the 4 source beams and 64 receiver elements is shown in Fig. 4 that shows three back-propagation images focused on the position of the echo-repeater for the low frequency data shown in this paper. The top panel shows the focus achieved by the 4 source beams, the middle panel by the 64 elements and the bottom panel the focus achieved by the product of the two. Although the resolution of the array was not able to be tested in this experiment due to the lack of reverberation and the presence of only one echo repeater, the numerical simulations suggest that sufficient resolution was present to resolve the echo repeater from bottom reverberation.

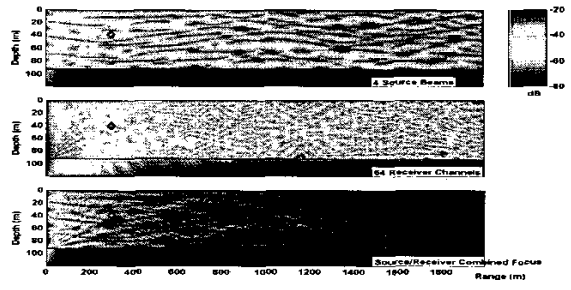

Fig. 4. Back propagation images from 4 source beams (top), 64 receiver elements (middle), and the combination (bottom).

D. Coherence Analysis

Fig. 5 shows $\sum_R \left| y\left(r_R, t\right) \right|^2$ the match-filtered signal incoherently averaged over the good elements of the vertical line array from the first transmission sequence. Note that the signal has substantially decayed to the noise level within the 250 ms spacing. The range of the echo repeater was approximately 0.3 km. This figure shows that the analysis window should be commensurate with 250 ms in order to capture the whole channel response.

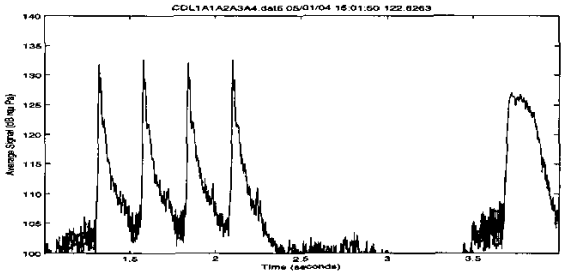

Fig. 5. Echoes from first transmission sequence. The echo repeater signal after 3.5 s is for another experiment.

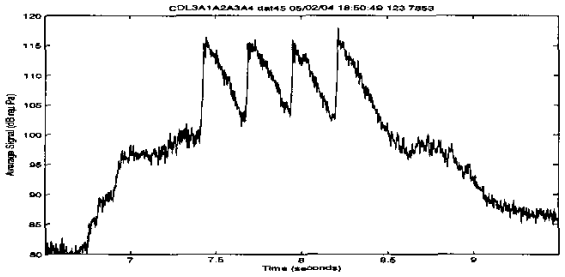

Fig. 6. Echoes from the third transmission sequence.

Fig. 6 shows the summed signal from the third transmission sequence. The range of the echo is 3.8 km. Note that the decay rate is substantially slower, but there is still significant decay in the 250 ms between transmissions.

In order to construct the data matrix $p\left(\vec{r}_R, \vec{r}_S, t\right)$, time-delayed replicas are assigned to different source indices

$$p\left(\vec{r}_R, \vec{r}_S, t\right) = y\left(\vec{r}_R, t - ST\right), \quad S = 0,1,2,3 \,. \tag{3.1}$$

The signal for the four source indices is shown in Fig. 5. This sequence of time-shifts aligns the four signals at approximately 2.1 s, but produces three sidelobes before and three sidelobes afterward.

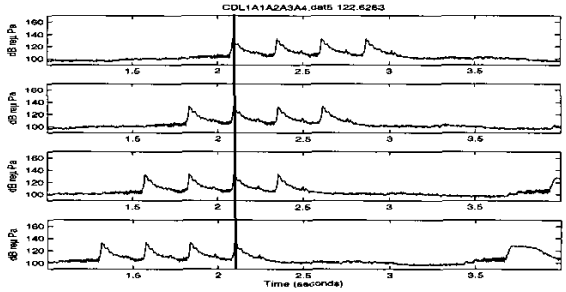

Fig. 7. Time shifted data from the first transmission sequence.

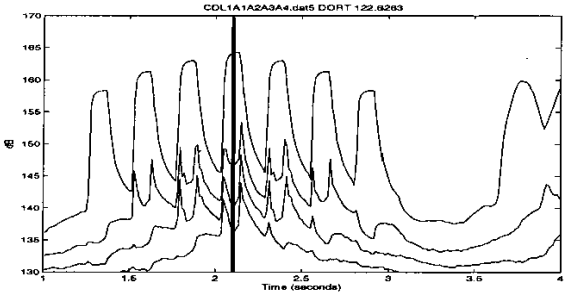

Fig. 8. Singular values from 0.5 to 1.0 kHz data for transmission sequence #1.

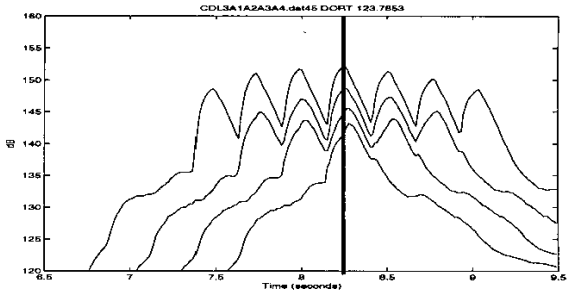

Fig. 9. Singular values of 3.0 to 3.5 kHz data for transmission sequence #3.

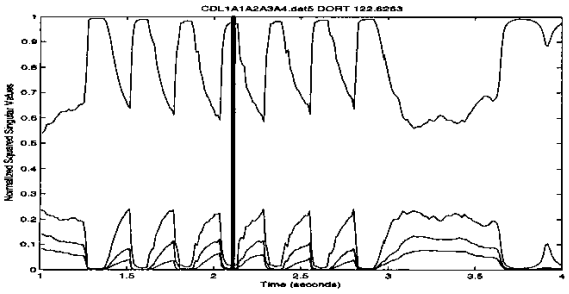

Fig. 10. Mean-squared normalized singular values of 0.5 to 1.0 kHz data for transmission sequence #1.

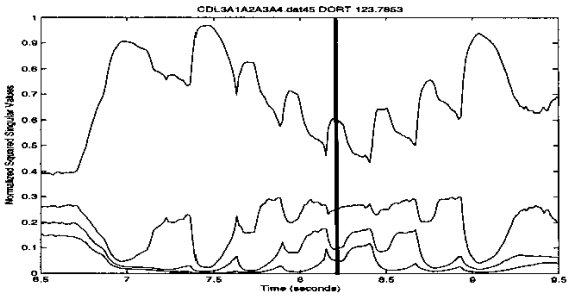

Fig. 11. Mean-squared normalized singular values from 3.0 to 3.5 kHz data for transmission sequence #3.

This data matrix is analyzed with a 100 ms Hanning-shaded, 1/8 overlap time window to produce smooth time behavior. The data matrix is Fourier transformed into the frequency domain and decomposed with SVD as in (2.19). The resulting singular values are inverse Fourier transformed into the time-domain and $s(n,m,t=0)$ are plotted in Fig. 8 for all four singular indices $n=1,2,3,4$ versus epoch $mT/8$. The singular values are evaluated at $t=0$ s, the location of the maximum in "short time".

Clearly there are a set of seven peaks in the first singular value as a function of time. The first peak and last peak occur when only one transmission is present across the source indices. The second and next-to-last occur when there are two source transmissions and the center peak occurs when all four transmissions are present. The central peak is higher because there is a greater amount of signal energy present due to the presence of all four source transmissions. The levels of the second, third and fourth singular values are slightly greater in the center. The significance of this increase can be seen through comparison with the theoretical predictions shown in Fig. 2. The SNR of the data shown in Fig. 5 is approximately 20 dB; at this SNR there is very little deviation in the noise singular values caused by mixing with the signal. Therefore, this increase is probably caused by decorrelation between the four identical transmissions due to motion of the SRA and echo repeater.

A greater decorrelation is expected at higher frequencies and greater ranges; and this is seen in the data from 3.0 to 3.5 kHz. Fig. 9 shows a steady increase in the lowest three singular values as the center of the pattern is approached. A comparison between the 0.5 to 1.0 kHz data in Fig. 8 and that in Fig. 9 shows the significant leakage of the signal into even the lowest singular value.

These singular values are **not** spaced as random noise is spaced however. This can be seen in the mean-square normalized singular values at 8.2 s shown in Fig. 11.

The theoretical singular values for Gaussian white noise have values of [0.34, 0.27, 0.22, 0.17]. In Fig. 11 the values of the singular values at 6.5 s where only noise is present shows values that differ slightly from those predictions. This difference is probably due to the correlations due to directionality of the noise field. The first peak in the first singular value is caused by noise emitted from the echo repeater. There is much more correlation present in this noise signal, causing a depression of the lowest three singular values. The center peak where all four signals are present has a singular spectrum of [0.65, 0.22, 0.10, 0.05] which differs significantly from the values to be expected for signals that are completely decorrelated.

Even though the high frequency signals are not completely decorrelated, their significant decorrelation can be seen by comparing Fig. 11 with Fig. 10 that shows the low-frequency results. Note the uniformly high peaks of the first singular value and the depressed lower three singular values.

D. DORT Analysis

The preceding analysis used four identical transmissions that can be used to measure the time variability of the system. When independent source transmissions are made, the resulting normalized singular values shown in Figs. 12 and 13 differ very little from those in Figs. 10 and 11, respectively. In other words, having four distinct source beams did not appreciably degrade the rank-1 structure of the echo repeater signal. The primary cause of degradation is motion of the SRA and the echo repeater.

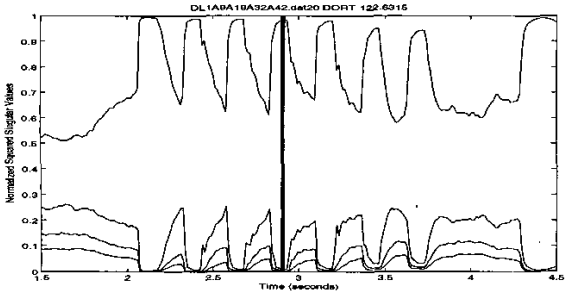

Fig. 12. Mean-squared normalized singular values from 0.5 to 1.0 kHz data for transmission sequence #2.

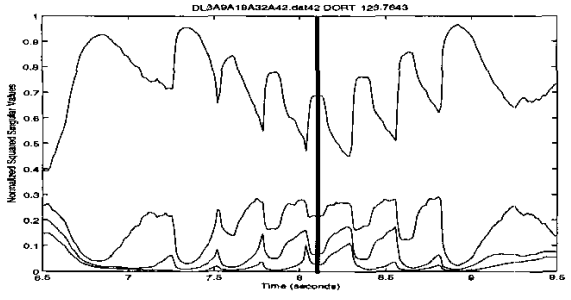

Fig. 13. Mean-squared normalized singular values of 3.0 to 3.5 kHz data for transmission sequence #4.

IV. Summary and Conclusions

Implementing DORT for shallow-water sonar raises several issues: coherence versus time-invariance, array-resolution versus separability-of-echoes, bandwidth and channel response, time-window duration and channel response, useful transmission signals and sequences and useful detection algorithms. This paper addresses only time-invariance and channel response. The data that was taken only had a single echo and no reverberation. Treating array-resolution versus separability-of-echoes requires a source powerful enough to generate reverberation or having more than one echo repeater.

The data collected and analyzed shows that sufficient time-invariance is attainable with a ship mounted source/receiver array, clearly at 0.5 to 1.0 kHz and even at 3.5 kHz if the lower coherence still allows sufficient separability-of-echoes. The sequence of pings occurred over a duration of approximately one second. Longer time delays can be expected to produce greater time-variability and greater spreading of the singular values from an individual scatterer.

Further development of DORT for shallow-water, bistatic sonars is required in the area of array resolution, transmission signals & sequences, and windowing techniques. This result is very encouraging for the further development of DORT for shallow-water, bistatic sonars.

Acknowledgments

C.F.G. and D.M.D. acknowledge many helpful conversations with M. Fink, C. Prada, T. Folegot, H.C. Song, W. Hodgkiss, W. Kuperman, D. Dowling, and A. Meyer. All of the authors thank the captains and crews of the R/V Endeavor and R/V Cape Henlopen for their expert help and flexibility. All the authors thank T.C. Yang, P. Gendron, J. Schindall, M. McCord, F. Erskine and R. Soukup for their technical assistance.

REFERENCES

[1] C. Prada, S. Manneville, D. Spoliansky, and M. Fink, "Decomposition of the time reversal operator: Detection and selective focusing on two scatterers," *J. Acoust. Soc. Amer.*, vol. 99, pp. 2067-2076, April 1996.

[2] T.D. Mast, A.I. Nachman, and R.C. Waag, "Focusing and imaging using eigenfunctions of the scattering operator," *J. Acoust. Soc. Amer.*, vol. 102, pp. 715-725, August 1997.

[3] G.F. Edelmann, T. Akal, W.S. Hodgkiss, W.A. Kuperman, and H.C. Song, , "An initial demonstration o funderwater acoustic communication using time reversal," IEEE Journal of Ocean. Eng., vol. 27, pp. 602-609, July 2002.

[4] H. Song, W.A. Kuperman, W.S. Hodgkiss, T. Akal, and P. Guerrini, "Demonstration of a high-frequency acoustic barrier with a time-reversal mirror," IEEE Journal of Ocean. Eng., vol. 28, pp. 246-249, April 2003.

[5] D.M. Fromm, C.F. Gaumond, J.F. Lingevitch, R.C. Gauss and R. Menis, "Detection in shallow water using broadband DORT," *J. Acoust. Soc. Amer.*, vol. 114, pp. 2399, October 2003.

[6] T. Folegot, W.A. Kuperman, H.C. Song, T. Akal and M. Stevenson, "Using acoustic orthogonal signal in shallow water time-reversal applications," *J. Acoust. Soc. Amer.*, vol. 115, pp. 2468, May 2004.

[7] C. Prada, E. Kerbut, J.L. Thomas and M. Fink, "Imaging with the DORT method," *J. Acoust. Soc. Amer.*, vol. 113, pp. 2211, April 2003.

[8] G. Montaldo, M. Tanter, M. Fink, "Real time identification of several targets by iterative time reversal," *J. Acoust. Soc. Amer.*, vol. 112, pp. 2308, May 2001.

[9] D.M. Fromm and C.F. Gaumond, "Time-reversal operator applied to broadband active sonar," *J. Acoust. Soc. Amer.*, vol. 109, pp. 2296, May 2001.

[10] M. Mehta, *Random Matrices.* Boston, MA: Academic Press, 1991.